Desalination and Water Treatment
www.deswater.com

doi: 10.5004/dwt.2022.28147

252 (2022) 126–139
March

Removal of cesium and silver ions using copper hexacyanoferrate encapsulated with barium alginate from aqueous solutions

Dalia A. Fadel[a,*], Mohamed. M. Azab[b], Amal A. Mahmoud[b], M. Yusif Elkady[b], Abdel-Fattah F. Shaaban[b]

[a]*Reactors Department, Nuclear Research Center, Egyptian Atomic Energy Authority, P.O. 13759, Cairo, Egypt, email: dalia_shaaban@windowslive.com*
[b]*Chemistry Department, Faculty of Science, Benha University, Benha, Egypt, Tel. +201009437694; email: drmorsy2000@yahoo.com (M.M. Azab), Tel. +201221792651; email: amal.ahmed@fsc.bu.edu.eg (A.A. Mahmoud), Tel. +2010072413835; email: Mahmoudelkady679@gmail.com (M. Yusif Elkady), Tel. +201091174238; email: afshaaban@hotmail.com (A.-F. Shaaban)*

Received 9 August 2021; Accepted 3 January 2022

ABSTRACT

Spherical beads of copper hexacyanoferrate encapsulated with barium alginate (CuHCF)-BA have been prepared by ionotropic gelation of copper nitrate and potassium ferrocyanide with sodium alginate in the presence of $Ba(NO_3)_2$ solution. The composition, properties and morphology of the resulting ion exchanger composite have been characterized by Fourier-transform infrared spectroscopy, scanning electron microscopy, X-ray diffraction and thermogravimetric analysis. Batch technique was used to investigate the effects of several parameters such as solution pH, metal ions concentration, contact time and temperature on metal ions uptake. The results indicated that the prepared ion exchanger composite have high affinity towards silver and cesium ions. The ion exchange data have been clarified by Freundlich isotherm model rather than other isotherms such as Langmuir and Temkin for silver ion while the results obtained of cesium ion was best fit with Langmuir isotherm model. Kinetics data have been analyzed using pseudo-first-order and pseudo-second-order and intra-particle diffusion equations. The result revealed that pseudo-second-order kinetic model was best fit with the obtained data for Ag^+ and Cs^+. Thermodynamic characteristics show that metal ion exchange process on the (CuHCF)-BA composite is both spontaneous and endothermic for Ag^+, while Cs^+ is not spontaneous but endothermic.

Keywords: Copper hexacyanoferrate; Ion exchanger; Barium alginate; Morphology; Isotherms; Kinetics; Thermodynamics; Cesium; Silver

1. Introduction

The treatment of radionuclide wastewater is in urgent need after the Fukushima Daiichi nuclear disaster. 137-cesium (^{137}Cs) has attracted great concern because of its long half-life and high solubility in water. The Cs^+ ion exhibits a low tendency to form complexes with ligands and high energy gamma ray emission [1–3] which can cause adverse effects on the environment and human health. ^{137}Cs can be easily incorporated into living organisms where it is deposited in the soft tissues, leading to cancer [4–5]. Therefore, development of new methods for the removal of cesium from wastewater is important in view of the environmental risks. The results revealed that the CMC-KCuFC adsorbent may be used in a wide pH range (5–10). As an effective biosorbent for cesium Cs^+ ion removal from wastewater, a composite potassium copper ferrocyanide particle adsorbent (CMC-KCuFC)

* Corresponding author.

based on carboxymethyl cellulose (CMC) was developed. The results revealed that the CMC-KCuFC adsorbent may be used in a wide pH range (5–10). The Freundlich isotherm model described the cesium adsorption process [6]. Polyaniline titanotungstate has been prepared by incorporation of polyaniline into the inorganic precipitate of titanotungstate. The comparison between inorganic materials and composite indicated that selectivity of Cs^+ ions by composite material is better than the inorganic one and suggested that chemisorption's were the predominant mechanism [7]. The sorption of Cs^+ from near neutral solutions using nickel–potassium ferrocyanide (along with other ferrocyanides) has been studied; the sorbent is selective to Cs^+ even in the presence of high concentrations of Na(I), K(I), Rb(I) or NH_4^+. The pseudo-second-order rate equation fits well kinetic profiles [8]. Prussian blue encapsulated in alginate beads reinforced with highly dispersed carbon nanotubes were prepared for the safe removal of cesium ions from aqueous solutions by batch and fixed bed column methods. Fixed bed adsorption column analysis indicated that the beads can be used for large scale treatment of cesium contaminated water [9]. Copper ferrocyanide (CuFC) was used to remove cesium. This was demonstrated by results of Jar test and Lab-scale which revealed that the adsorption capacity of CuFC was better than that of potassium zinc hexacyanoferrate. The concentration of cesium in the effluent decreased with the operation time, which reflected that the used adsorbent retained its adsorption capacity. Also, the results showed that the experimental values fitted well with the calculated values in the CTA-MF process. [10]. A new method was employed using immobilization of transition metals (such as cobalt, nickel, and copper) in nanosized carboxylic latex emulsions for the preparation of colloid stable selective sorbents for cesium uptake. The sorption capacities of the colloid sorbents based on mixed potassium/transition metals ferrocyanides were in the range 1.3–1.5 mol Cs/mol ferrocyanide with the highest value found for the copper ferrocyanide [11]. El-Naggar et al. [12] reported that calcium alginate/graphene-sodium dodecyl sulfate (CA/GR-SDS) nanocomposite beads were synthesized, characterized and their sorption properties toward Cs^+ were evaluated. The highest sorbed Cs^+ amounts were acquired within the first 30 min of contact time. The pseudo-second-order model gave the best fitting of the experimental kinetic data. Simple thermodynamic models have been applied to the isotherm sorption data and the relevant thermodynamic parameters were determined from the graphical presentation of this mode [12]. The removal of cesium from an aqueous solution using $K_2Zn_3[Fe(CN)_6]_2$ by an adsorption–microfiltration (AMF) process was investigated in jar and lab-scale tests. The obtained cesium data in the jar test fit a Freundlich-type isotherm well. In the lab-scale test, the mean cesium concentration of the raw water and the effluent were 106.87 and 0.59 g L^{-1}, respectively, the mean removal of cesium was 99.44%. The removal of cesium in the lab-scale test was better than that in the jar test [13]. A fine crystalline ammonium tungstophosphate (AWP) exchanger with high selectivity towards Cs^+ was encapsulated in calcium alginate (CaALG). The selective separation and recovery of ^{137}Cs were investigated by the batch and column methods using real high-level liquid waste (HLLW) and simulated (SHLLW) . The breakthrough curve of Cs^+ had an S-shaped profile and the breakpoint increased with decreasing flow rate [14]. Adsorption isotherm studies of Cs^+ from aqueous solution using polyaniline titanotungstate (PATiW) are investigated and it was found that the polyaniline titanotungstate is highly selective to Cs^+ ion [15].

Heavy metal removal from natural water sources and industrial wastewater is of particular interest since they accumulate in living organisms and cannot be biodegraded, resulting in a variety of illnesses when levels surpass certain limits [16,17]. Humans, animals, and plants are all affected by high metal concentrations in solution. Metal cation contamination of water and soil rises in lockstep with the growth of industrial activity [18, 19]. Most recent studies have concentrated on the use of low-cost adsorbents to reduce processing costs for these industrial wastewaters treatment [20–22]. Precipitation, electrolysis, solvent extraction, ion-exchange resins, chelating agents, and other methods are now available for the removal of silver. When metal concentrations in effluents are sufficiently high, that is, over 0.93 mmol L^{-1}, these procedures can be employed commercially on a wide scale [23,24]. The majority of these procedures, however, are unsatisfactory due to the high cost, limited efficiency, and inapplicability of sludge disposal to a wide variety of contaminants [25]. Khan et al. used a batch method to investigate silver adsorption on bentonite. For sorption systems, distribution coefficients were calculated as a function of contact time, pH, sorbent and sorbate concentrations, and temperature [26]. Hanzlík et al. [27] examined the adsorption of Cd, Cu, and Ag from water using twelve carbonaceous materials by batch adsorption experiment. The adsorption process kinetics was highly quick for the first 5 h but very sluggish for the remaining 65 h. Rakchaiyawan et al. [28] investigated the use of chitosan-polyvinyl alcohol resin as a silver ion adsorbent. Kinetic tests in batches were carried out. The pseudo-second-order model was shown to be adequate for describing adsorption behavior. The aim of the present study is to prepare a copper hexacyanoferrate encapsulated with barium alginate and use it for the removal of Cs^+ and Ag^+ from aqueous solution using batch technique. The effects of various parameter like pH value, metal ion concentration, contact time and temperature on adsorption capacity of (CuHCF)-BA for cesium and silver ions will be studied using batch method and will be investigated using Langmuir, Freundlich and Temkin isotherms. Kinetic and thermodynamic parameters of studied metals removal were also estimated.

2. Materials and methods

2.1. Materials

Silver nitrate ($AgNO_3$), 99% and cesium nitrate ($CsNO_3$), 99% purchased from Sigma-Aldrich Co., USA and used in the ion exchange experiments. pH adjustments were carried out using 0.1 N nitric acid (HNO_3) and 0.1 N sodium hydroxide (NaOH). All Ag^+ and Cs^+ solutions were prepared with double distilled water Super purity nitric acid (SpA, 68%) purchased from Sigma-Aldrich Co.,

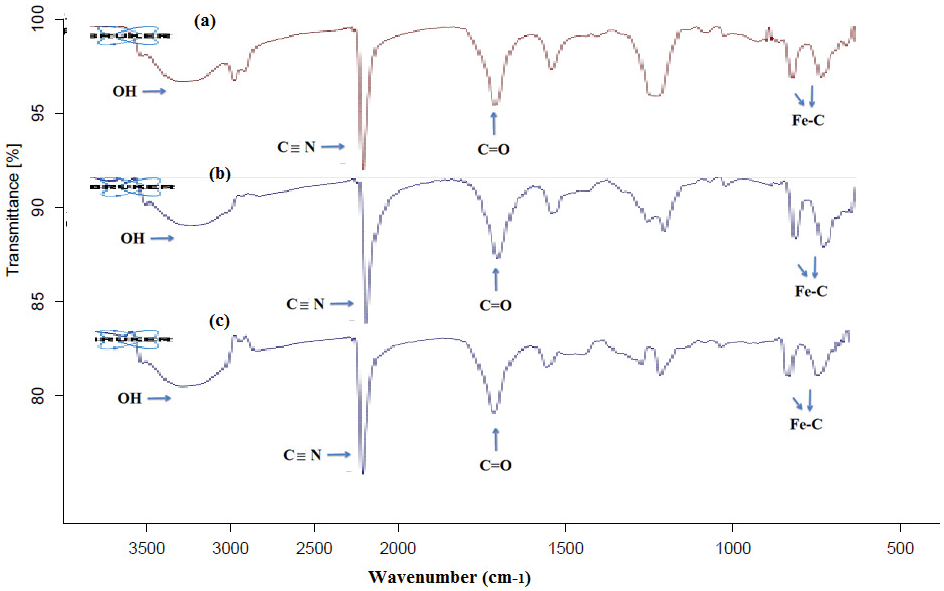

Fig. 1. FTIR spectrum of (a) the synthesized copper hexacyanoferrate (CuHCF)-BA composite, (b) loaded with Ag^+ ions and (c) Cs^+ ions.

USA. Potassium ferrocyanide (KFC), copper nitrate [$Cu(NO_3)_2{\cdot}3H_2O$] and sodium alginate were pure grade products of Merck Co., Germany and were used directly. Barium nitrate was purchased from Sigma-Aldrich Co., USA.

2.2. Synthesis

2.2.1. Synthesis of spherical beads of (CuHCF)-BA

2.2.1.1. Preparation of copper hexacyanoferrate [29]

Solution of potassium ferrocyanide (KFC) (167 mL, 0.1 M) was dropping on solution of $Cu(NO_3)_2{\cdot}3H_2O$ (500 mL, 0.1 M) slowly at room temperature with vigorous stirring then heating to 80°C in water bath for 4 h, then stop heating and stirring and leaves it to 24 h to make coagulation. Washing the precipitate about 8 times with total volume two liters of water then centrifuge the precipitate and dry at 60°C until give constant weight then ground the precipitate.

2.2.1.2. Preparation of (CuHCF)-BA

Added sodium alginate on copper hexacyanoferrate solution slowly with vigorous stirring for 24 h to form suspension solution and ensuring sodium alginate solubility. This solution was dropping into solution of $Ba(NO_3)_2$ (0.2 M) dissolved in distilled water using syringe with suitable needle 18G making slow flowing with slowly stirring. Leave the beads on stirring for 2 h then leave it for 2 d. Then, the beads were separated from the solution and washed with water several times and drying.

2.2.1.3. Regeneration

The elution process was performed by passing 300 mL of 2.0 M $Cu(NO_3)_2$ solution as eluent through a glass column at the flow rate of 5 mL min^{-1}. After each adsorption–desorption cycle, (CuHCF)-BA composite was again carefully washed several times with deionized water to regenerate for further experiment. To evaluate the reusability of (CuHCF)-BA, five cycles of adsorption–desorption experiments were performed. It is obvious that the adsorption capacity of (CuHCF)-BA was a little affected after the repeated five regeneration cycles, the adsorption capacity decreased from 100% to 88% after five cycles. These results indicate that, (CuHCF)-BA is a durable adsorbent and have a good ability to compete commercial adsorbents in terms of economic feasibility.

2.3. Instrumentation

2.3.1. Scanning electron microscopy

High resolution scanning electron microscope was used to observe the surface morphology and particle size of the ion exchanger resin synthesized. Micrographs were obtained using scanning electron microscopy (SEM QUANTA FEG 250 with field emission gun, FEI Company-Netherlands) micro analyzer microscope. The samples were prepared by deposition of a thin gold film, sputtered using a Balzer SCD 050 deposition system.

2.3.2. Fourier-transform infrared spectroscopy measurements

The IR spectrum of the ion exchanger was measured using Fourier-transform infrared spectroscopy (ATR-FTIR) BRUKER, Vertex 80 (Germany) Spectrophotometer in the range 4,000–400 cm^{-1} with resolution 4 cm^{-1}.

2.3.3. Thermogravimetric analysis

Thermal analysis experiments including thermogravimetric analysis (TGA) and differential scanning calorimetry

(DSC) for the ion exchanger were carried out using SDTG 600, USA Thermogravimetric analyzer. The experiment was performed in a dynamic atmosphere of nitrogen from room temperature to 900°C at heating rate of 10°C/min.

2.3.4. X-ray diffraction

The X-ray diffraction of ion exchanger in powder form was obtained from PANalytical X'Pert Pro target Cu Kα radiation with secondary monochromator Holland radiation (λ = 1.540 Å). The scanning range was between angle 2θ = 0–60 for ion exchanger.

2.3.5. Determination of the metal ions concentration

Metal ions concentration was determined by using Hitachi atomic absorption Z-6100 polarized Zeeman spectrometer.

2.4. Uptake of metal ions

2.4.1. Uptake of metal ions by batch method

All experiments were performed with 0.1 g resin in 250 mL bottles with 100 mL of single metal ion solution on a temperature controlled shaker at 200 rpm. All experiments were carried out at 25°C except the temperature experiments. The desired pH of solution was adjusted using few drops of 0.1 M HNO_3 and 0.1 M NaOH solutions. Concentration of the metal ions in the solution was determined by atomic absorption). Experiments were carried out in triplicate. The adsorption capacity was calculated according to Eq. (1):

$$q = \frac{(C_0 - C_e)V}{W} \quad (1)$$

where Q_e is the adsorption capacity (mmol g^{-1}). C_0 and C_e are the initial and the equilibrium concentrations of metal ions (mmol L^{-1}), respectively. V is the volume of metal ions solution (L) and W is the weight of dry resin (g). Determination of the optimum pH for adsorption of metal ions, were carried out by shaking 0.1 g of resin with 100 mL (1.47 mmol L^{-1}) metal ion solution for 1 h at adjusted pH for Ag^+ and (2 mmol L^{-1}) metal ion solution for 2 h at adjusted pH for Cs^+ ion. Experiments of adsorption isotherms were performed by shaking 0.1 g of resin with 100 mL of metal ion solution at optimum pH in a concentration ranging from 0.74 to 10.59 (mmol L^{-1}) after 1 h of shaking for Ag^+ and from 0.37–1.32 mmol L^{-1} for Cs^+ after 2 h of shaking, the resin was filtered and the remaining metal ion concentration in solution was estimated. To investigate the adsorption kinetic of the adsorption process, 0.1 g of resin and 100 mL of metal ion solution was continuously shaken at optimum pH and concentration at 25°C. The flasks containing the mixtures were withdrawn at different time intervals to determine the remaining concentration of metal ions. Measurement of metal ion adsorption by the resin as a function of temperature was studied in the temperature range of 25°C–40°C. Experiments were performed by shaking 0.1 g of resin with 100 mL of metal ion solutions (1.07 mmol L^{-1}) for silver and (1.108 mmol L^{-1}) for cesium under the optimum pH and contact time. After adsorption, the residual concentration of metal ion was determined as described earlier.

3. Results and discussion

3.1. Characterization of (CuHCF)-BA

3.1.1. FTIR spectrum

Fig. 1a–c show FTIR spectrum of the synthesized copper hexacyanoferrate (CuHCF)-BA beads, beads captures Ag^+ ions and beads captures Cs^+, respectively, which showed characteristic peak at 3,350 cm^{-1} attributed to OH stretching [29], band at 1,598 cm^{-1} for COOH stretching, 1,053 cm^{-1} corresponding for C–O–C stretching and sharp peak at 2,096 cm^{-1} related to C≡N stretching. The bands in the 474–610 cm^{-1} region are due to the (Fe–C) stretching [30].

3.1.2. Thermal gravimetric analysis (TGA)

The thermogravimetric method was used to assess the beads thermal stability and water content. Under nitrogen atmosphere, a known amount of surface-dried swollen beads was heated in an aluminium crucible at a heating rate of 10°C/min. Fig. 2 shows the TG of the beads. The loss of absorbed water molecules causes a massive weight loss in the TG at 31°C, which continues up to 180°C, resulting in a total weight loss of 28%. Then, from 180°C to 230°C, the second degradation phase was seen, with a total weight loss of 5% owing to CO_2 evolution. The third stage, which reflects skeletal alginate chain structure degradation, was found between 230°C and 350°C. Finally, due to cyanide breakdown and metal oxide, the fourth stage occurs between 375 and 790. The mass was left as a residue at the end of 905°C.

3.1.3. X-ray diffraction

CuKα radiation was used to record the X-ray powder diffraction pattern of the produced (CuHCF)-BA-alginate beads (Fig. 3). The diffraction pattern revealed wide diffraction peaks, suggesting that the CuHCF particles are crystalline. The major diffraction peaks were found at 17.69°, 25.25°, and 36.13°, which are quite similar to those seen in $Cu_2[Fe(CN)_6 \cdot xH_2O]$ (JCPDS card number 00-023-0213). The existence of crystalline CuHCF in the synthesised beads was verified.

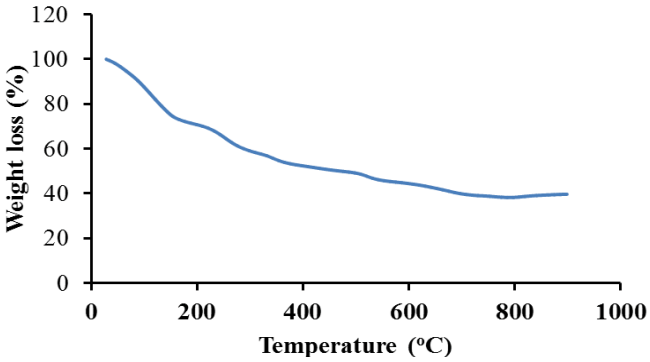

Fig. 2. TGA of the synthesized (CuHCF)-BA composite.

3.1.4. Scanning electron microscopy–energy-dispersive X-ray spectroscopy

The surface morphology of the resin was examined by scanning electron microscopy and energy-dispersive X-ray microanalysis (EDX) system. The scanning electron micrograph images of the synthesized (CuHCF)-BA beads and beads captures Ag^+ ions and beads captures Cs^+ are shown in Fig. 4a–c, respectively. The morphology of (CuHCF)-BA beads before metal ion uptake showed thick surface. After metal ion uptake, the beads surface became totally covered by silver ions adsorption and more shrinkage with Cs^+. The presence of silver ions and cesium ion in the synthesized (CuHCF)-BA beads were confirmed from EDX measurements (Fig. 4b and c). In Fig. 4b and c the ion exchanger (CuHCF)-BA beads showed a new distinct signals at 3.0 and 3.2 keV attributed to Ag^+ ions, whereas two distinct signals at 4.25 and 4.75 keV attributed to Cs^+ ions. The objective of this analysis was to map elemental Ag^+ and Cs^+ ions qualitatively (not quantitatively) on the composite surface. However, the level of the Ag^+ signal observed was sufficient for providing a qualitative idea of the homogeneous distribution of Ag^+ element at the surface of the sorbent: the percentage (in mass) of Ag^+ was 45.13% while Cs^+ 1.35%. From the obtained results, this confirmed the following suggested mechanism of the ion exchange reaction between substituted copper with silver and also cesium ions in (CuHCF)-BA beads.

$$Cu_2Fe(CN)_6 + 2M^+ \rightarrow CuM_2\,Fe(CN)_6 + Cu^{2+}$$

where $M^+ = Ag^+$ or Cs^+. Also, the obtained results showed that the ion exchange capacity of silver ions higher than the ion exchange capacity of cesium ions. This means that silver ion ability to exchange with copper is higher than cesium ion as illustrated in the previous other researches results [31,32].

3.2. Batch method for metal ion uptake

3.2.1. Effect of pH on metal ions uptake

The influence of the pH on the uptake capacity of silver ion Ag^+ was examined by batch system at 25°C in the pH range of 1–7.0 and the results are presented in Fig. 5a.

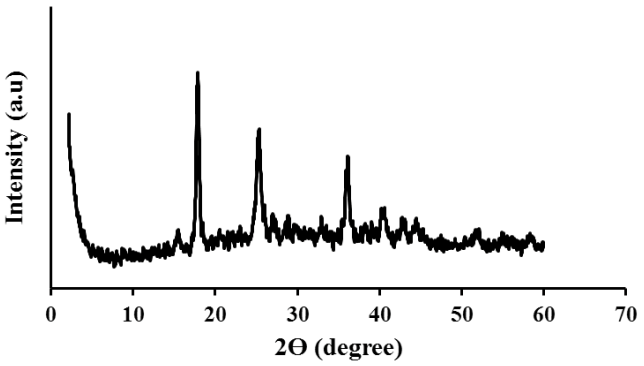

Fig. 3. X-ray diffraction of the synthesized (CuHCF)-BA composite.

The results showed that the capacity increased when the pH level was raised till it reached its highest point (optimum value). The pH value that resulted in the maximum metal ion exchange capacity was found to be 7.0. All subsequent tests were carried out at the optimal pH for silver ions. Metal was transformed to precipitated metal hydroxide above optimal pH, and the ion exchange of these ions could not be reliably quantified. Because the cesium ion exhibits a plateau between pH 6 and 10 at 25°C, tests were carried out at pH 7 (Fig. 5b).

3.2.2. Effect of initial concentration of metal ions

The influence of the initial Ag^+ ion of concentrations on equilibrium ion exchange was performed at initial concentrations range from 0.74 to 10.59 mmol L^{-1} at 25°C, shaking time 1 h and pH 7 for the sorption of Ag^+ ions on (CuHCF)-BA resin and the results are illustrated in Fig. 6a. The results showed that the amount of Ag^+ ions loaded onto (CuHCF)-BA resin increased as the initial concentration of silver ions increased. The results showed that the maximum ion exchange capacity of Ba-alginate resin not detected with this concentration range.

For cesium ion The influence of the initial ion concentrations on equilibrium ion exchange was performed at initial concentrations range from 0.37 to 1.32 mmol L^{-1} at 25°C, shaking time 2 h and pH 7 for the ion exchange of Cs^+ ions on (CuHCF)-BA composite and the results are illustrated in Fig. 6b. The results showed that the amount of Cs^+ loaded onto (CuHCF)-BA increased as the initial concentration of cesium ions increased. The results showed that the maximum ion exchange capacity of Ba-alginate resin 0.48 mmol g^{-1}.

3.2.2.1. Isotherm models for ion exchange process

Langmuir, Freundlich, and Temkin isotherm models were used to evaluate equilibrium isotherm data. The Langmuir isotherm model is expressed in its linear form as [33].

$$\frac{C_e}{q} = \frac{C_e}{Q_{\max}} + \frac{1}{K\,Q_{\max}} \tag{2}$$

where C_e is the equilibrium concentration of metal ions (mmol L^{-1}), q is the equilibrium adsorption capacity (mmol g^{-1}), $Q_{\max}$ (mmol g^{-1}) and K (L $mmol^{-1}$) are the maximum ion exchange capacity and binding constant, respectively. With the slope and intercept of the linearized plot of C_e/q_e vs. C_e (Fig. 7a for silver ion and Fig. 7b for cesium ion). Table 1 lists the parameters of the Langmuir model that were computed.

The separation factor (R_L) is a dimensionless parameter in the Langmuir isotherm model [34], which is expressed as follows:

$$R_L = \frac{1}{1 + KC_o} \tag{3}$$

The Langmuir constant (binding constant) is K, while the starting metal ion concentration (mmol L^{-1}) is C_o.

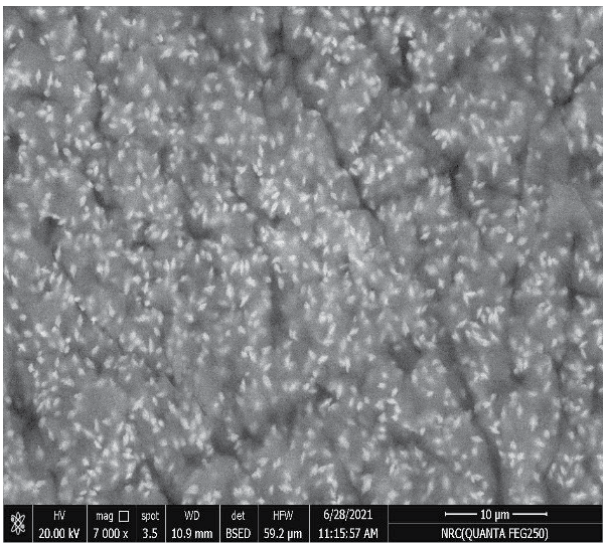

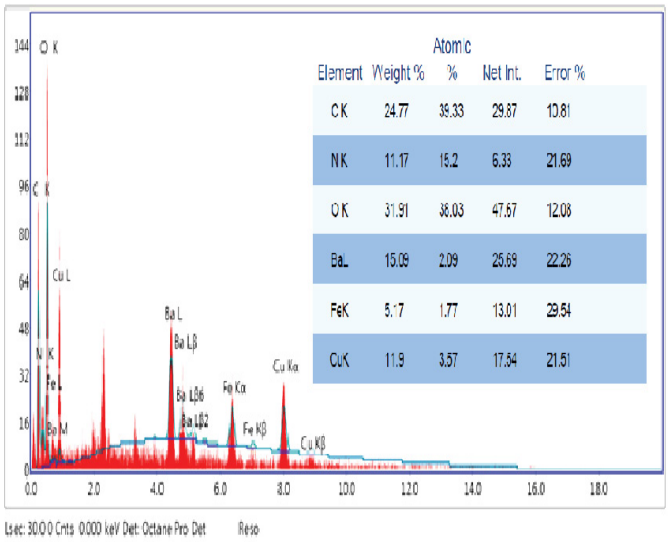

(a)

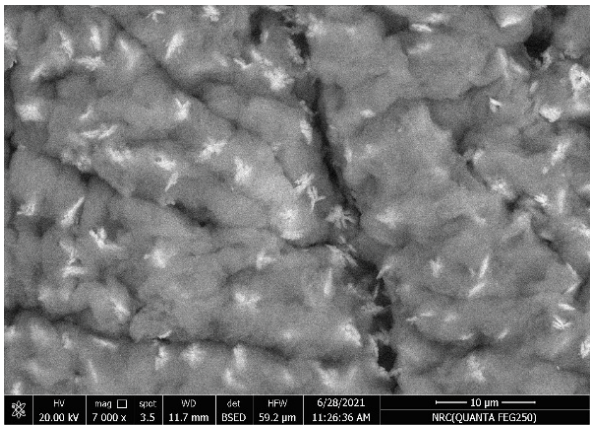

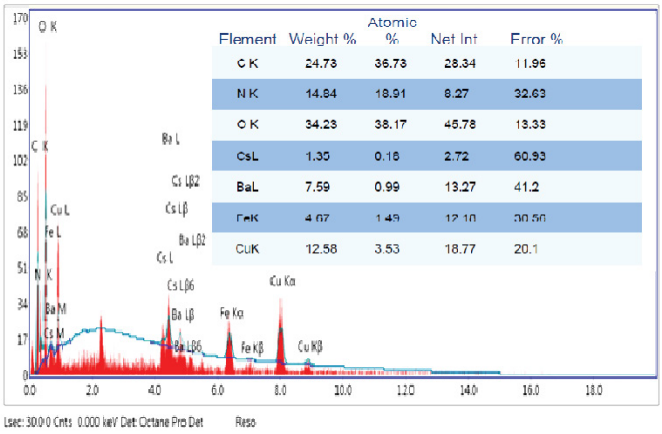

(b)

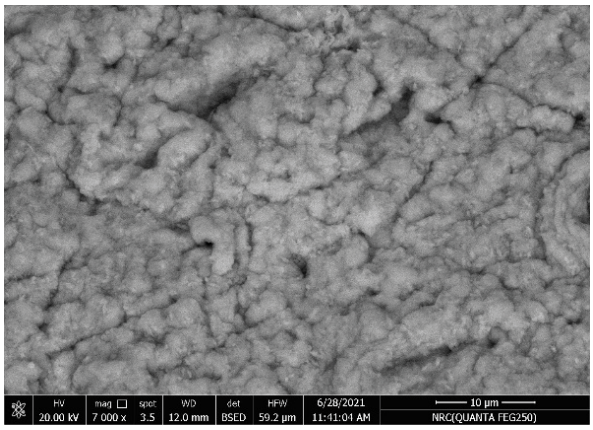

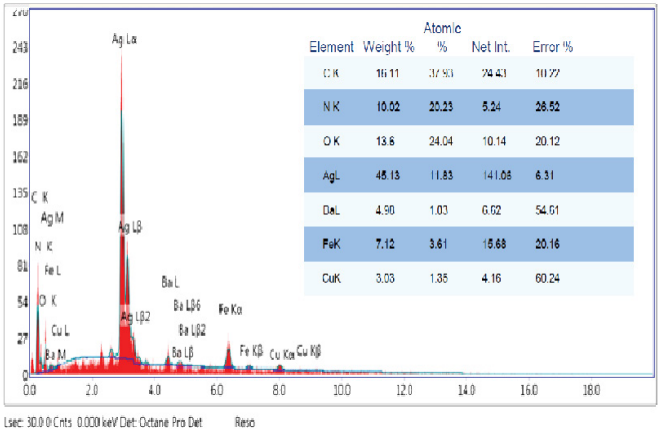

(c)

Fig. 4. SEM-EDX of (a) (CuHCF)-BA composite, (b) (CuHCF)-BA composite with Cs^+ ions and (c) (CuHCF)-BA composite with Ag^+ ions.

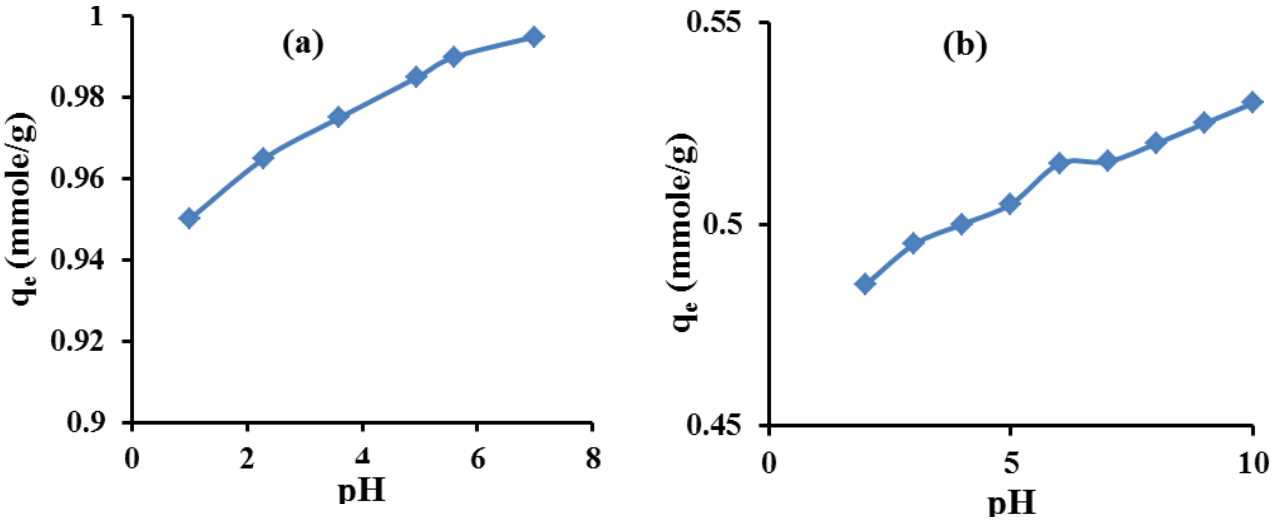

Fig. 5. Effect of pH on the amount of sorbent of (a) Ag^+ ions and (b) Cs^+ ions on (CuHCF)-BA composite at 25°C.

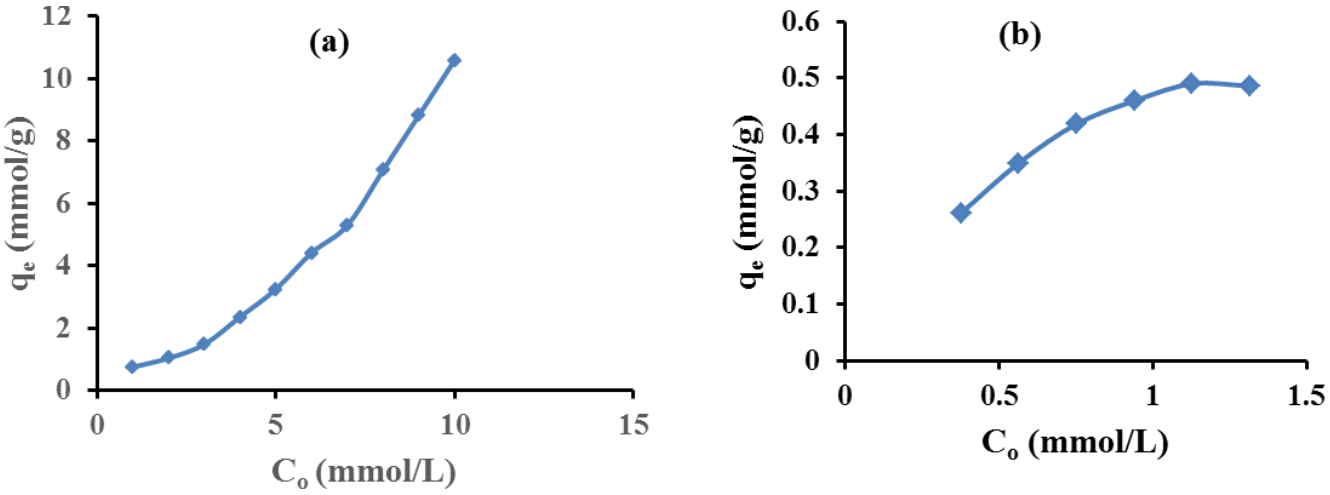

Fig. 6. Effect of initial concentration of (a) Ag^+ ions and (b) Cs^+ ions on (CuHCF)-BA composite at 25°C and pH 7.

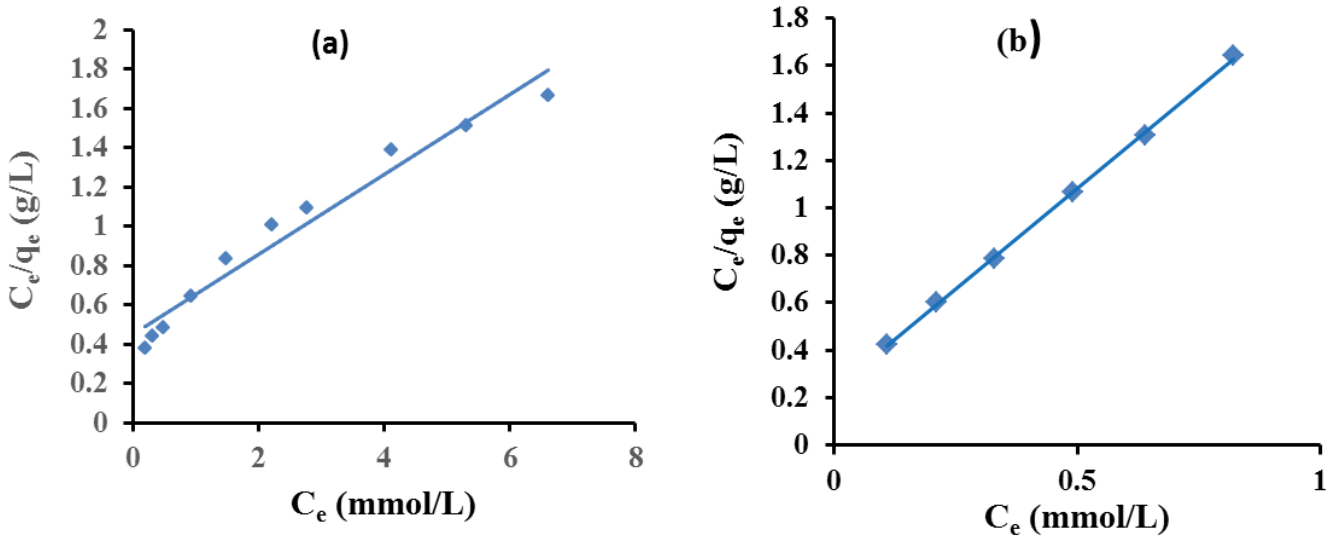

Fig. 7. Langmuir adsorption isotherm of (a) Ag^+ ions and (b) Cs^+ on (CuHCF)-BA composite at 25°C.

The computed value of R_L suggests that the isotherm's form should be unfavourable ($R_L > 1$), linear ($R_L = 1$), favorable ($0 < R_L < 1$), or irreversible ($R_L = 0$) [35, 36].

where K is the Langmuir constant (binding constant) and C_o is the initial concentration of metal ion (mmol L^{-1}). The value of R_L which was calculated recommends the shape of the isotherm to be unfavorable ($R_L > 1$), linear ($R_L = 1$), favourable ($0 < R_L < 1$), or irreversible ($R_L = 0$) [35, 36]. Fig. 8 shows a plot of R_L vs. C_o. The calculated values of R_L for metal ions were between zero and one, indicating that metal ion exchange on Ba-alginate composite was favourable. The R_L values dropped when the C_o of metal ions rose for both metal ions, as shown in Fig. 9a for silver and Fig. 8b for cesium, indicating that metal ion adsorption was more effective at higher starting metal ion concentrations.

Freundlich's isotherm model is based on empirical data. The Freundlich isotherm model is represented by the following equation [37]:

$$\log q_e = N \log C_e + \log K_F \quad (4)$$

where q_e denotes the equilibrium capacity (mmol g^{-1}), C_e is the equilibrium concentration of metal ion (mmol L^{-1}), and K_F and N denote the Freundlich constants for the capacity and its efficiency, respectively. When $\log q_e$ was plotted against $\log C_e$, a straight line with slope N and intercept $\log K_F$ was obtained (Fig. 9a for silver and Fig. 9b for cesium). The values of K_F and N were calculated and are collected in Table 1. The value of term N in the Freundlich isotherm model presented isotherms can be unfavourable ($N > 1$), favourable ($0 < N < 1$), or irreversible ($N = 0$). For all metal ions, the values computed for N range from 0 to 1, indicating that the ion exchange process of metal ions through composite is simple.

The Temkin isotherm model is represented by the following equation [38]:

$$q_e = B \ln K_T + B \ln C_e \quad (5)$$

The heat of ion exchange process and the equilibrium binding constant, are represented by the Temkin constants B and K_T, respectively. The values of B and K_T were obtained from the slope and intercept of linear plot of q_e vs. $\ln C_e$ (Fig. 10a for silver ion and Fig. 10b for cesium ion) and shown in Table 1. As shown in Table 1 the good fit experimental data with Langmuir, Freundlich, and Temkin isotherm models and high correlation coefficient (R^2) obtained for these plots indicated the validity of these models to Ba-alginate composite for Ag^+ and Cs^+ ions. But Freundlich equation showed better results than Temkin and Langmuir models because of higher correlation coefficient for Ag^+ ions and Langmuir model for Cs^+ ions.

Table 1
The parameters of Langmuir, Freundlich and Temkin isotherms for (CuHCF)-BA composite at 25°C

Isotherms	Parameters	Ag^{+1}	Cs^{+1}
Langmuir	Q_{max} (mmol g^{-1})	4.9	0.55
	K (L $mmol^{-1}$)	0.455	7.26
	R^2	0.962	0.9995
Freundlich	K_F (mmol L^{-1})	1.4	0.0210
	N	0.56	0.329
	R^2	0.996	0.9611
Temkin	B	0.948	0.123
	K_T	6.12	81.45
	R^2	0.95	0.9846

3.2.3. Influence of contact time on ion exchange process

In order to determine the effect of contact time of (CuHCF)-BA resin in aqueous solution for Ag^+ ion at (pH 7, 25°C and 1.07 mmol L^{-1}) and for Cs^+ ion at (pH 7, 25°C and 1.108 mmol L^{-1}) variations of adsorption capacity (q_e) vs. time (0.25–3 h) were plotted, as shown in Fig. 11a for Ag^+ a nd Fig. 11b for Cs^+. It is observed that the ion exchange of Ag^+ and Cs^+ ions from aqueous solution using the composite was continuously increased with time increase until reaching equilibrium between two phases after 2.5 h. Therefore,

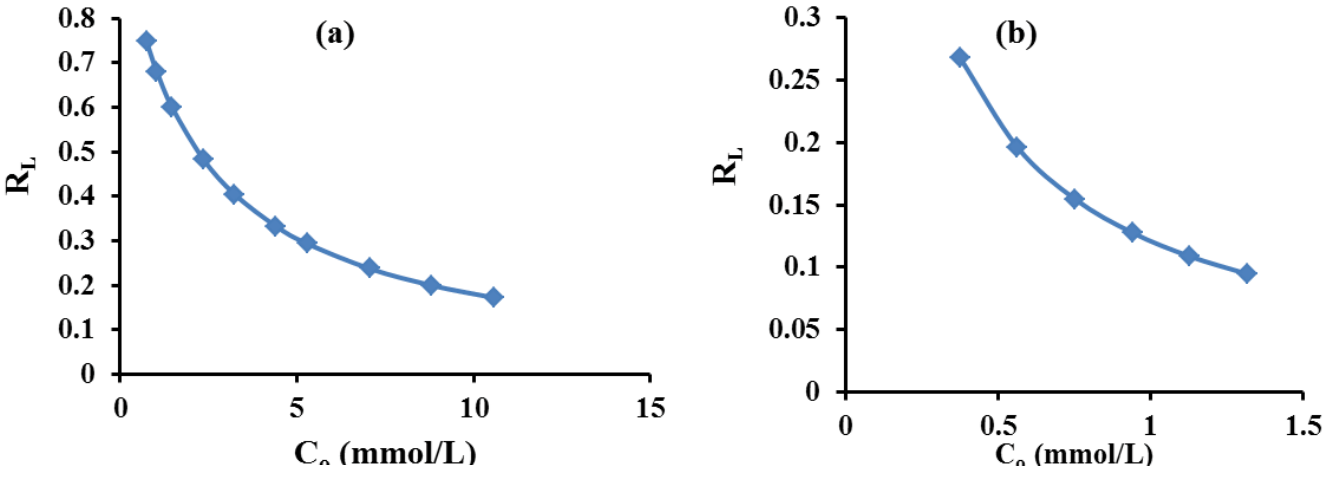

Fig. 8. Variation of adsorption intensity (R_L) with (a) initial silver ion concentration (C_o) and (b) initial cesium ion concentration (C_o).

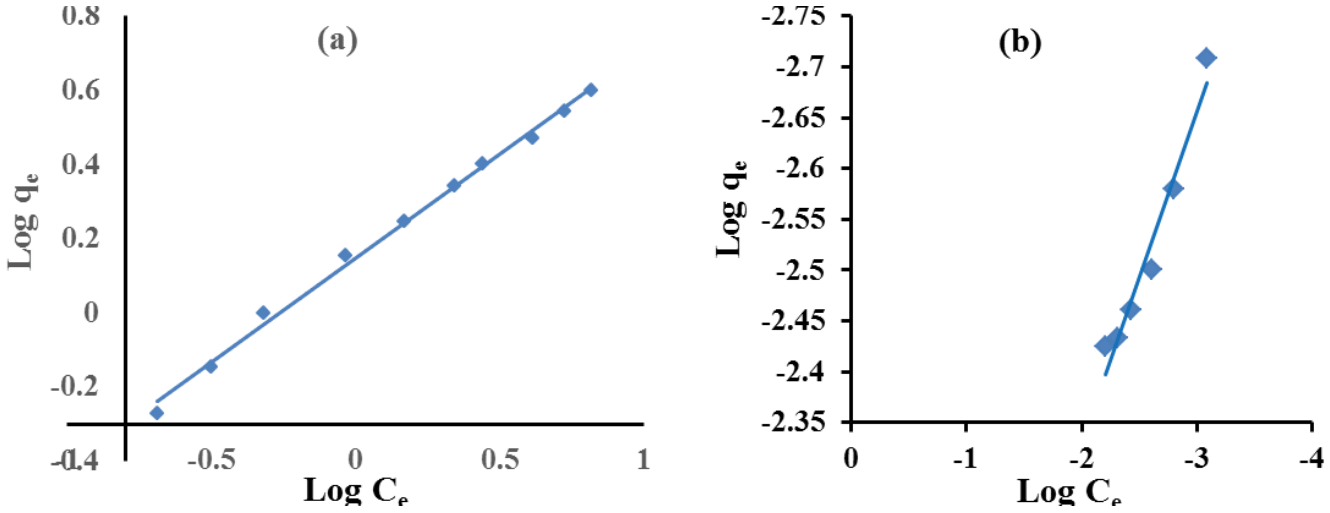

Fig. 9. Freundlich adsorption isotherm of (a) Ag^+ ions and (b) Cs^+ ions on (CuHCF)-BA composite at 25°C.

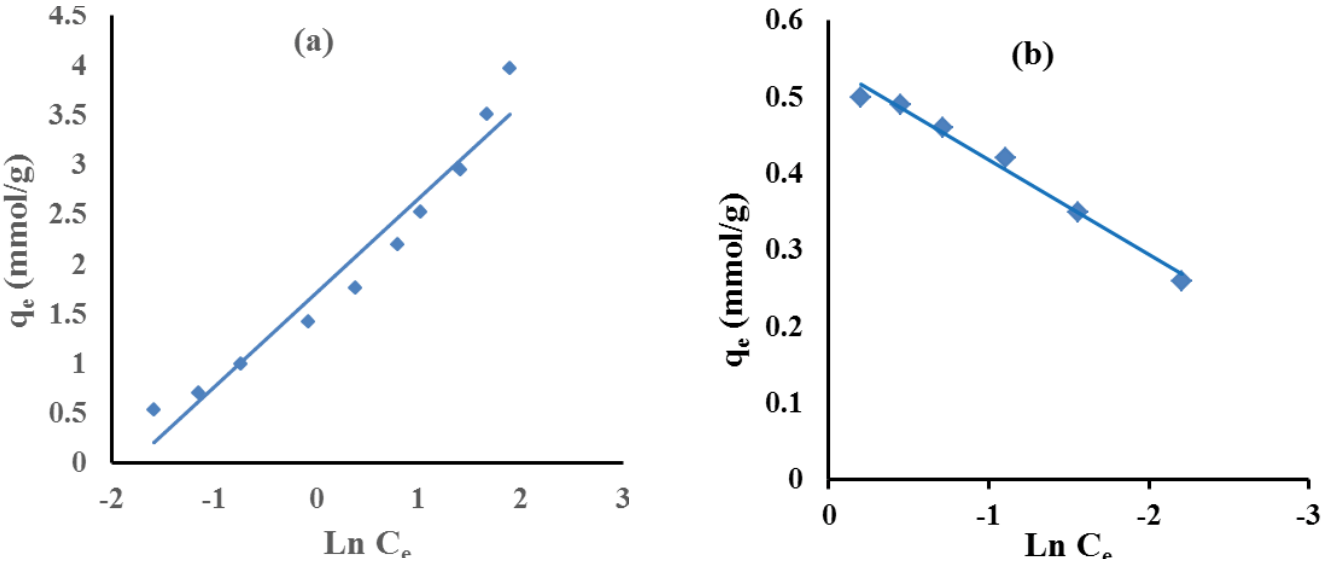

Fig. 10. Temkin adsorption isotherm of (a) Ag^+ ions and (b) Cs^+ ions on (CuHCF)-BA composite at 25°C.

this obtained equilibrium time was selected for the next adsorption experiments.

3.2.3.1. Ion exchange kinetic models

The ion exchange results were used to investigate the kinetic mechanism which controls the ion exchange process. The most widely used models of Lagergren's pseudo-first-order; pseudo-second-order and intra particle diffusion were used to investigate the kinetic process [39–40]. The linear form of the first order rate equation by Lagergren and Svenska [41] is expressed in Eq. (6):

$$\log\left(q - q_t\right) = \log q - \left(\frac{K_{ads}}{2.303}\right)t \tag{6}$$

where q_e is the ion exchange capacity (mmol g^{-1}) at equilibrium and q_t is the ion exchange capacity (mmol g^{-1}) at time t (h). The Lagergren rate constant (h^{-1}) of ion exchange is K_{ads}. The sorption of Ag^+ and Cs^+ ions at different periods was plotted using Eq. (6) as shown in Fig. 12a for Ag^+ and Fig. 12b for Cs^+. Table 2 contains the Lagergren constants. The pseudo-second-order model was also applied to the experimental data. In linearized form, Ho's pseudo-second-order model might be stated as follows:

$$\frac{t}{q_t} = \frac{1}{K_2 q^2} + \left(\frac{1}{q}\right)t \tag{7}$$

where K_2 (g $mmol^{-1}$ h^{-1}) is the pseudo-second-order rate constant. The kinetic plot of t/q_t vs. t for Ag^+ ions sorption was presented in Figs. 13a and b for Cs^+ The relationship was linear, and the value of the correlation coefficient (R^2) as shown in Table 2. Table 2 lists the constants for the second-order kinetic model graphs. The correlation

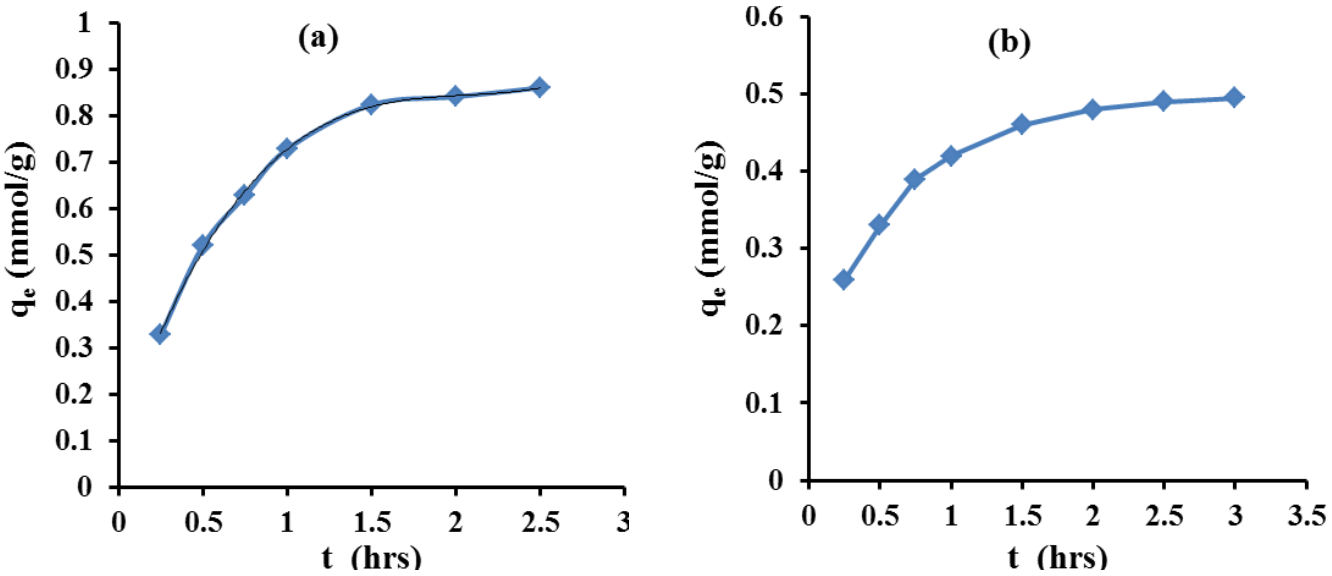

Fig. 11. Effect of contact time of (CuHCF)-BA composite in aqueous solution of (a) Ag^+ ion at (pH 7, 25°C and 1.07 mmol L^{-1}) and (b) Cs^+ ion at (pH 7, 25°C and 1.108 mmol L^{-1}.

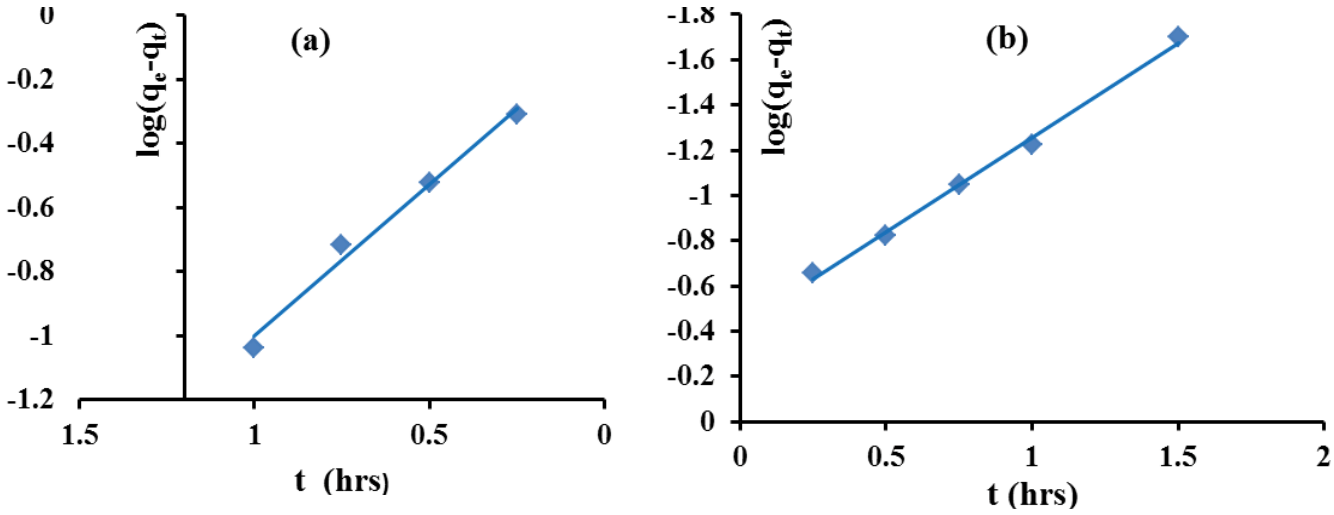

Fig. 12. The first-order kinetic plot of (CuHCF)-BA composite in aqueous solution of (a) Ag^+ ion and (b) Cs^+ ion.

coefficient value (R^2) of the second-order kinetics was obviously greater than the value obtained from the first-order kinetics, as can be shown in Table 2. As a result, the sorption of Ag^+ and Cs^+ ions on (CuHCF)-BA composite follows second-order kinetics.

Weber and Morris [42] introduced Eq. (8) to explain the intraparticle diffusion concept.

$$q_t = K_{id} t^{0.5} \tag{8}$$

where K_{id} (mmol g^{-1} $h^{-0.5}$) is the intraparticle diffusion rate constant. K_{id} was calculated by plotting q_t vs. $t^{0.5}$ (Fig. 14a for silver and Fig. 14b for cesium). Table 2 lists the constants used in these visualisations. According to Weber and Morris, the metal ion could be transported from the aqueous phase to the composite in three ways: (a) Diffusion of metal ions through the boundary layer to the surface of the composite; (b) Intra-particle diffusion: migration of metal ions from the outside surface of the composite to the inside holes or pores of the composite through pore diffusion; or (c) intraparticle diffusion; migration of metal ions. With respect to Eq. (8), if the plot gives a straight line, intraparticle diffusion is accepted as the only rate-limiting step, but multi-linearity is formed which refers to two or more stages related to the adsorption of metal ions [43]. It was found the plot gives a straight line (Fig. 14). Depend on these results obtained; we can conclude that the intraparticle diffusion was the only step of rate-limiting step.

3.2.4. Thermodynamics parameters of ion exchange

Ion exchange experiments were carried out at various temperatures (25°C, 30°C, 35°C, and 40°C) to investigate the

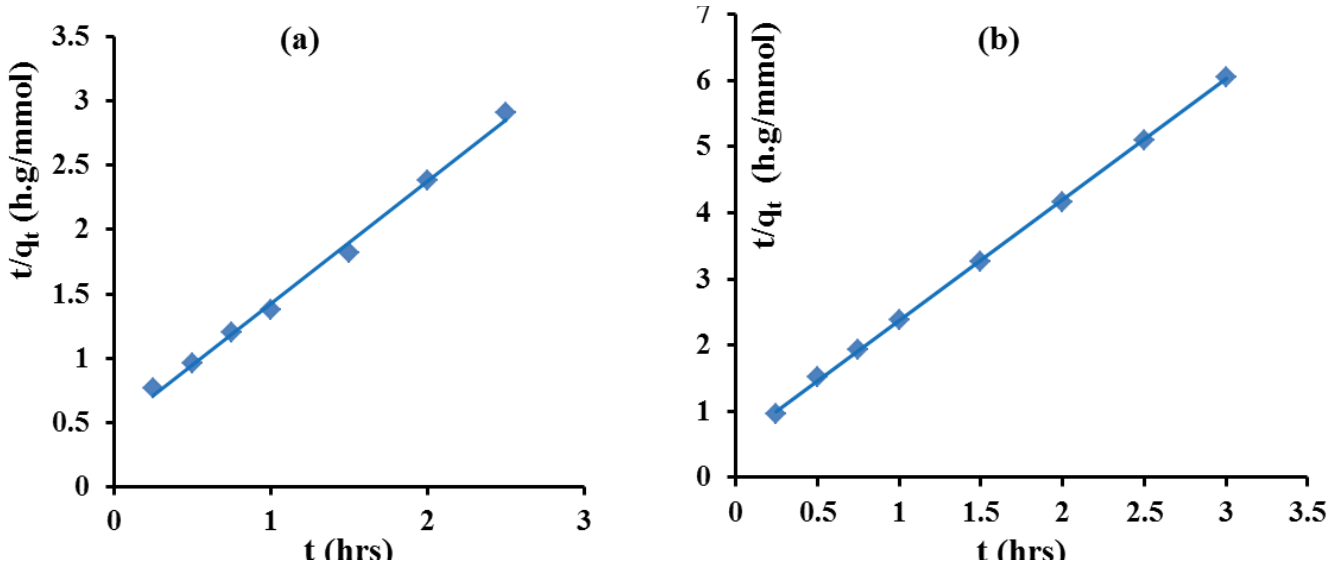

Fig. 13. The second-order kinetic plot of (CuHCF)-BA composite in aqueous solution of (a) Ag^+ ion and (b) Cs^+ ion.

Table 2
Kinetic parameters for the adsorption of silver and cesium on (CuHCF)-BA composite

Kinetic models	Parameters	Ag^+	Cs^+
Pseudo-first-order	K_1 (h^{-1})	2.19	1.92
	R^2	0.986	0.9956
	q_e(theoretical) (mmol g^{-1})	0.88	0.38
Pseudo-second-order	K_2 (g $mmol^{-1}$ h^{-1})	1.9	6.15
	R^2	0.996	0.9997
	q_e(theoretical) (mmol g^{-1})	1.05	0.547
	Q(experimental) (mmol g^{-1})	0.85	0.48
Intraparticle diffusion model	K_{id} (mmol g^{-1} $h^{-0.5}$)	0.586	0.1853
	R^2	0.968	0.9025

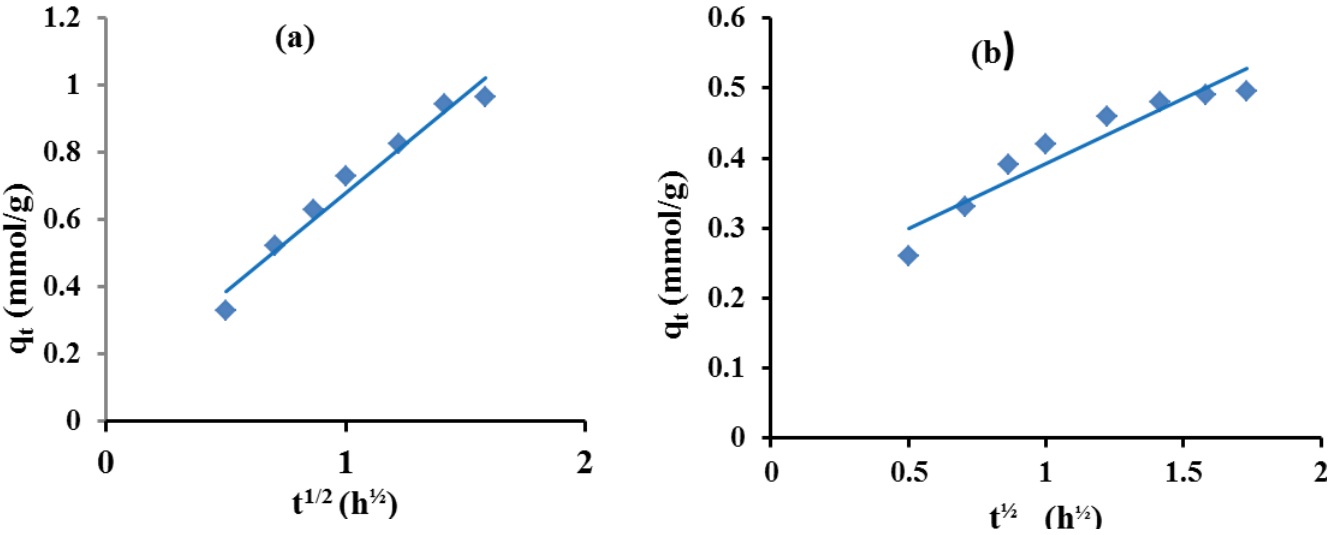

Fig. 14. Weber–Morris intraparticle diffusion model of (CuHCF)-BA composite in aqueous solution of (a) Ag^+ ion and (b) Cs^+ ion.

thermodynamic characteristics of the ion exchange process. Equilibrated with 0.1 g of Ba-alginate composite at optimal pH value. Metal ion solution (100 mL, 1.07 mmol L^{-1}) for silver ion and (100 mL, 1.108 mmol L^{-1}) for cesium ion. Eq. (9) [44] was used to obtain the equilibrium distribution coefficient (K_d) for the ion exchange process.

$$K_d = \frac{C_o - C_e}{C_e} \times \frac{V}{W} \tag{9}$$

where C_o and C_e denote the initial and equilibrium concentrations of metal ions in aqueous solution (mmol L^{-1}), V denotes the total volume of the solution (L), and W denotes the weight of the (CuHCF)-BA composite (g). Plotting $\ln K_d$ vs. $1/T$ according to Eq. (10) (Fig. 15a for Ag^+ and Fig. 15b for Cs^+) yielded the typical enthalpy change (ΔH°_{ads}) and entropy change (ΔS°_{ads}) of the ion exchange process.

$$\ln K_d = \frac{\Delta S^\circ_{ads}}{R} - \frac{\Delta H^\circ_{ads}}{RT} \tag{10}$$

where R is the gas constant, which is 8.314 J mol^{-1} K^{-1}. The slope and intercept values (Fig. 15a for Ag^+ and Fig. 15b for Cs^+) correspond to ΔH°_{ads} and ΔS°_{ads}, respectively.

This following equation was used to determine the free energy change of adsorption (ΔG°_{ads}):

$$\Delta G^\circ = -RT \ln K_d \tag{11}$$

Table 3 shows the thermodynamic characteristics for metal ion adsorption onto Ba-alginate resin including ΔG°_{ads}, ΔH°_{ads}, and ΔS°_{ads}. Negative values of ΔH°_{ads} indicated that metal ion adsorption was an exothermic process, as seen in Table 3 [45,46]. Additionally, greater unpredictability owing to the release of H_2O during hydration during the adsorption of metal ions may be linked with positive values of ΔS°_{ads} [47, 48]. Finally, the thermodynamic parameters revealed that the adsorption process is continuous, as evidenced by negative ΔG°_{ads} values for Ag^+ but not for Cs^+ which has a positive value for ΔG°_{ads}.

3.2.5. Comparison with other adsorbents

Table 4 shows the results of comparing the adsorption capacity of various cesium adsorbents [49–53] to that of the (CuHCF)-BA composite. It was evident that the produced composite had a significantly greater ion exchange capacity than other cesium adsorbents. More importantly, this composite was made at room temperature utilizing only environmentally benign and low-cost ingredients. As a result, the (CuHCF)-BA composite proved a cost-effective cesium removal material.

Table 5 shows the highest adsorption capacities for Ag^+ removal from aqueous solutions reported by several adsorbents [54–59]. The (CuHCF)-BA composite bead was discovered to have a greater ion exchange capacity than certain other adsorbents. The (CuHCF)-BA resin composite beads may be utilized as effective ion exchange for Ag^+ removal from aqueous solution, as indicated by this finding.

4. Conclusion

Ionotropic gelation of copper nitrate, potassium ferrocyanide, and sodium alginate in the presence of barium nitrate solution produced spherical beads of current composite. FTIR, SEM, TGA, and X-ray diffraction were used to evaluate the composite's composition, characteristics,

Table 3
Thermodynamic parameters for silver and cesium adsorption on (CuHCF)-BA composite

Parameter	Ag^+	Cs^+
ΔH° (J mol^{-1})	979 (J mol^{-1})	81.94 (J mol^{-1})
ΔS° (JK^{-1} mol^{-1})	3.38 (JK^{-1} mol^{-1})	0.2426 (JK^{-1} mol^{-1})
Temp. (K)	$-\Delta G^\circ$ (J mol^{-1})	ΔG° (J mol^{-1})
298	28.2	9.645
303	45.1	8.432
308	62	7.219
313	78.9	6.006

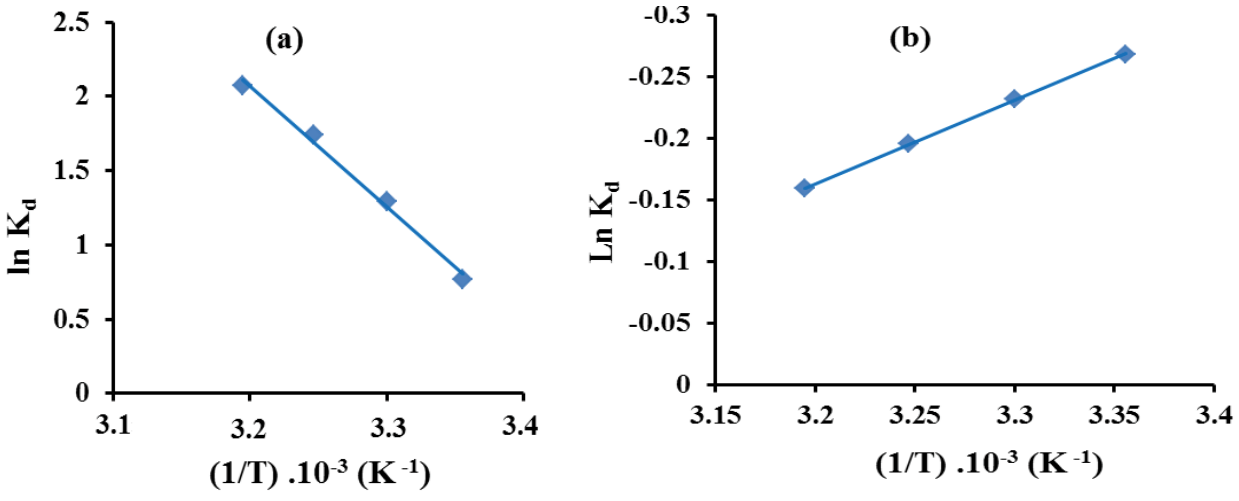

Fig. 15. The effect of temperature on the distribution coefficient of (a) Ag^+ ions and (b) Cs^+ ions onto (CuHCF)-BA composite.

Table 4
Comparison of maximum adsorption capacity of adsorbents reported in literature for Cs^+ adsorption

Adsorbent	pH	T (K)	Q_{max} (mg g^{-1})	References
Whisker-supported composite	6	298.15	32.9	[49]
Pre-treated area shell biomass	5.5	–	3.93 ± 0.11	[50]
Prussian blue modified magnetite	–	–	16.2	[51]
Nickel hexacyanoferrate–walnut shell	–	298.15	4.94 ± 0.5	[52]
Nanocrystalline mordenite	–	298.15	37.3	[53]
CMC-KCuFC particles	4–10	298.15	60.827	[6]
CMC-Cu	4–10	298.15	7.85	[6]
(CuHCF)-BA	7	298.15	73.15 (0.55 mmol g^{-1})	This study

Note: '—' represented the information was not given in the references.

Table 5
Comparison among adsorption of different adsorbents for Ag^+

Adsorbent	Adsorption capacity (mg g^{-1})	Reference
RH	1.62	[54]
EP	8.46	[55]
CTS/MMT	43.48	[56]
CTS/BC	52.91	[57]
Mn-MV	69.2	[58]
IGCC	89.2	[59]
(CuHCF)-BA	528.56 (4.9 mmol g^{-1})	This study

and shape. For Ag^+ and Cs^+, this composite has a high ion exchange capacity. It was observed that the (CuHCF)-BA composite bead had a higher ion exchange capacity than other adsorbents. The (CuHCF)-BA composite beads might be used as an ion exchanger for the removal of Cs^+ and Ag^+ from aqueous solutions. Several variables impacted metal ion sorption onto (CuHCF)-BA, including solution pH, metal ion concentration, contact duration, and solution temperature. The current sorption pH for Ag^+ and Cs^+ ions in batch technique was 7. The ion exchange process for Ag^+ followed Freundlich isotherm model, while the ion exchange process for Cs^+ was followed Langmuir isotherm model. The exchange mechanism was shown to suit the pseudo-second-order model effectively in kinetic studies. Thermodynamic characteristics show that metal ion exchange on the (CuHCF)-BA composite is both spontaneous and endothermic for Ag^+, while Cs^+ is not spontaneous but endothermic. By batch technique, the (CuHCF)-BA composite was effective in removing Ag^+ and Cs^+.

References

[1] R. Yi, G. Ye, F.C. Wu, M. Wen, X. Feng, J. Chen, Highly efficient removal of ^{137}Cs in seawater by potassium titanium ferrocyanide functionalized magnetic microspheres with multilayer core-shell structure, RSC Adv., 4 (2014) 37600–37608.

[2] E. Calabrese, Improving the scientific foundations for estimating health risks from the Fukushima incident, Proc. Natl. Acad. Sci. U.S.A., 108 (2011) 19447–19448.

[3] C. Dwivedi, A. Kumar, J.K. Ajish, K.K. Singh, M. Kumar, P.K. Wattal, P.N. Bajaj, Resorcinol-formaldehyde coated XAD resin beads for removal of cesium ions from radioactive waste: synthesis, sorption and kinetic studies, RSC Adv., 2 (2012) 5557–5564.

[4] R.R. Sheha, Synthesis and characterization of magnetic hexacyanoferrate (II) polymeric nanocomposite for separation of cesium from radioactive waste solutions, J. Colloid Interface Sci., 388 (2012) 21–30.

[5] T. Sangvanich, V. Sukwarotwat, R.J. Wiacek, R.M. Grudzien, G.E. Fryxell, R.S. Addleman, C. Timchalk, W. Yantasee, Selective capture of cesium and thallium from natural waters and simulated wastes with copper ferrocyanide functionalized mesoporous silica, J. Hazard. Mater., 182 (2010) 225–231.

[6] Y. Zong, Y. Zhang, X. Lin, D. Ye, D. Qiao, S. Zeng, Facile synthesis of potassium copper ferrocyanide composite particles for selective cesium removal from wastewater in the batch and continuous processes, RSC Adv., 7 (2017) 31352–31364.

[7] I.M. El-Naggar, E.S. Zakaria, I.M. Ali, M. Khalil, M.F. El-Shahat, Kinetic modeling analysis for the removal of cesium ions from aqueous solutions using polyaniline titanotungstate, Arabian J. Chem., 5 (2012) 109–119.

[8] C. Vincent, A. Hertz, T. Vincent, Y. Barré, E. Guibal, Immobilization of inorganic ion-exchanger into biopolymer foams application to cesium sorption, Chem. Eng. J., 236 (2014) 202–211.

[9] A.K. Vipin, B. Hu, B. Fugetsu, Prussian blue caged in alginate/calcium beads as adsorbents for removal of cesium ions from contaminated water, J. Hazard. Mater., 258–259 (2013) 93–101.

[10] F. Han, G.-H. Zhang, P. Gu, Removal of cesium from simulated liquid waste with countercurrent two-stage adsorption followed by microfiltration, J. Hazard. Mater., 225–226 (2012) 107–113.

[11] V. Avramenko, S. Bratskaya, V. Zheleznov, I. Sheveleva, O. Voitenko, V. Sergienko, Colloid stable sorbents for cesium removal: preparation and application of latex particles functionalized with transition metals ferrocyanides, J. Hazard. Mater., 186 (2011) 1343–1350.

[12] M.R. El-Naggar, E.A. El-Sherif, R.M. Maree, H.S. Mekhamer, Batch and fixed bed column investigations of the sorptive removal of cesium ions from aqueous solutions using modifed graphene-alginate nanocompositebeads, J. Radiat. Res. Appl. Sci., 14 (2021) 146–158.

[13] C.-P. Zhang, P. Gu, J. Zhao, D. Zhang, Y. Deng, Research on the treatment of liquid waste containing cesium by an adsorption–microfiltration process with potassium zinc hexacyanoferrate, J. Hazard. Mater., 167 (2009) 1057–1062.

[14] H. Mimura, Y. Wu, W. Yufei, Y. Niibori, I. Yamagishi, M. Ozawa, T. Onishi, S. Koyama, Selective separation and recovery of cesium by ammonium tungstophosphate-alginate microcapsules, Nucl. Eng. Des., 241 (2011) 4750–4757.

[15] I.M. El-Naggar, E.S. Zakaria, I.M. Ali, M. Khalil, M.F. El-Shahat, Chemical studies on polyaniline titanotungstate and its uses to reduction cesium from solutions and polluted milk, J. Environ. Radioact., 112 (2012) 108–117.

[16] A. Heidari, H. Younesi, Z. Mehraban, Removal of Ni(II), Cd(II), and Pb(II) from a ternary aqueous solution by amino

functionalized mesoporous and nano mesoporous silica, Chem. Eng. J., 153 (2009) 70–79.
[17] J.P. Chen, L. Wang, Characterization of metal adsorption kinetic properties in batch and fixed-bed reactors, Chemosphere, 54 (2004) 397–404.
[18] K.N. Ghimire, H. Kai, K. Inoue, K. Ohto, H. Kawakita, H. Harada, M. Morita, Heavy metal removal from contaminated scallop waste for feed and fertilizer application, Bioresour. Technol., 99 (2008) 2436–2441.
[19] H. Aydın, Y. Bulut, C. Yerlikaya, Removal of copper(II) from aqueous solution by adsorption onto low-cost adsorbents, J. Environ. Manage., 87 (2008) 37–45.
[20] E.-S.Z. El-Ashtoukhy, N.K. Amin, O. Abdelwahab, Removal of lead(II) and copper(II) from aqueous solution using pomegranate peel as a new adsorbent, Desalination, 223 (2008) 162–173.
[21] C. Chen and J. Wang, Removal of Pb^{2+}, Ag^{+}, Cs^{+} and Sr^{2+} from aqueous solution by Brewery's waste biomass, J. Hazard. Mater., 151 (2008) 65–70.
[22] A.K. Meena, K. Kadirvelu, G.K. Mishra, C. Rajagopal, P.N. Nagar, Adsorptive removal of heavy metals from aqueous solution by treated sawdust (*Acacia arabica*), J. Hazard. Mater., 150 (2008) 604–611.
[23] A. Kapoor, T. Viraraghavan, D. Roy Cullimore, Removal of heavy metals using the fungus *Aspergillus niger*, Bioresour. Technol., 70 (1999) 95–104.
[24] B. Volesky, In: R. Amils, A. Ballester, Ed., Biohydrometallurgy and the Environment Toward the Mining of the 21st Century, Part B, Elsevier, Amsterdam, 1999, pp. 143–152.
[25] M.A. Barakat, New trends in removing heavy metals from industrial wastewater, Arabian J. Chem., 4 (2011) 361–377.
[26] S.A. Khan, Riaz-ur-Rehman, M. Ali Khan, Adsorption of chromium (III), chromium (VI) and silver (I) on bentonite, J. Waste Manage., 15 (1995) 271–282.
[27] P. Hanzlík, J. Jehlička, Z. Weishauptová, O. Šebek, Adsorption of copper, cadmium and silver from aqueous solutions onto natural carbonaceous material, Plant Soil Environ., 50 (2004) 257–264.
[28] U. Rakchaiyawan, Y. Kulratkitiwong, K. Piyamongkala, Kinetics adsorption of silver ion by blend chitosan-polyvinyl alcohol resin, Int. J. Environ. Sci. Dev., 6 (2015) 655–659.
[29] A. Nilchi, R. Saberi, M. Moradi, H. Azizpour, R. Zarghami, Adsorption of cesium on copper hexacyanoferrate-PAN composite ion exchanger from aqueous solution, Chem. Eng. J., 172 (2011) 572–580.
[30] Z. Du, M. Jia, X. Wang, Cesium removal from solution using PAN-based potassium nickel hexacyanoferrate (II) composite spheres, J. Radioanal. Nucl. Chem., 298 (2013) 167–177.
[31] F. Adekola, M. Fedoroff, S. Ayrault, C. loos-Neskovic, E. Garnier and L.T. Yu, Interaction of silver ions in solution with copper hexacyanoferrate(II) $Cu_2Fe(CN)_6$, J. Solid State, 132 (1997) 399–406.
[32] S. Ayrault, B. Jimenez, E. Garnier, M. Fedoroff, D.J. Jones, C. Loos-Neskovic, Sorption mechanisms of cesium on $Cu_2Fe(CN)_6$ and $Cu_3[Fe(CN)_6]_2$ hexacyanoferrates and their relation to the crystalline structure, J. Solid State Chem., 141 (1998) 475–485.
[33] V. Kourim, J. Rais, B. Million, Exchange properties of complex cyanides. I. Ion exchange of caesium on ferrocyanides, J. Inorg. Nucl. Chem., 26 (1964) 1111.
[34] C.M. Futalan, C.-C. Kan, M.L. Dalida, C. Pascua, M.-W. Wan, Fixed-bed column studies on the removal of copper using chitosan immobilized on bentonite, Carbohydr. Polym., 83 (2011) 697–704.
[35] I. Langmuir, The adsorption of gases on plane surfaces of glass, mica and platinum, J. Am. Chem. Soc., 40 (1918) 1361–1403.
[36] T.W. Weber, R.K. Chakravot, Pore and solid diffusion models for fixed bed adsorbents, AIChE J., 20 (1974) 228–238.
[37] A. Sari, M. Tuzen, D. Citak, M. Soylak, Equilibrium, kinetic and thermodynamic studies of adsorption of Pb(II) from aqueous solution onto Turkish kaolinite clay, J. Hazard. Mater., 149 (2007) 283–291.
[38] X.-S. Wang, J. Huang, H.-Q. Hua, J. Wang, Y. Qin, Determination of kinetic and equilibrium parameters of the batch adsorption of Ni(II) from aqueous solutions by Na-mordenite, J. Hazard. Mater., 142 (2007) 468–476.
[39] H. Freundlich, Adsorption in solution, Phys. Chem. Soc., 40 (1906) 1361–1368.
[40] M.J. Temkin, V. Phyzev, Recent modifications to Langmuir isotherms, Acta Physiochim. U.S.S.R., 12 (1940) 217–222.
[41] Y.S. Ho, Citation review of Lagergren kinetic rate equation on adsorption reactions, Scientometrics, 59 (2004) 171–177.
[42] Y.S. Ho, Review of second-order models for adsorption systems, J. Hazard. Mater., 136 (2006) 681–689.
[43] W.J. Weber, J.C. Morris, Equilibria and capacities for adsorption on carbon, J. Sanitary Eng. Div., 90 (1964) 79–108.
[44] C. Sarici-Ozdemir, Y. Onal, Equilibrium, kinetic and thermodynamic adsorptions of the environmental pollutant tannic acid onto activated carbon, Desalination, 251 (2010) 146–152.
[45] A. Nilchi, R. Saberi, M. Moradi, H. Azizpour, R. Zarghami, Adsorption of cesium on copper hexacyanoferrate–PAN composite ion exchanger from aqueous solution, Chem. Eng. J., 172 (2011) 572–580.
[46] S.M. El-Bahy, Z.M. El-Bahy, Synthesis and characterization of a new iminodiacetate chelating resin for removal of toxic heavy metal ions from aqueous solution by batch and fixed bed column methods, Korean J. Chem. Eng., 33 (2016) 2492–2501.
[47] S.M. El-Bahy, Z.M. El-Bahy, Synthesis and characterization of polyamidoxime chelating resin for adsorption of Cu(II), Mn(II) and Ni(II) by batch and column study, J. Environ. Chem. Eng., 4 (2016) 276–286.
[48] M.-C. Fournier-Salaun, P. Salaun, Quantitative determination of hexavalent chromium in aqueous solutions by UV-Vis spectrophotometer, Cent. Eur. J. Chem., 5 (2007) 1083–1093.
[49] T. Sasaki, S. Tanaka, Magnetic separation of cesium ion using Prussian blue modified magnetite, Chem. Lett., 41 (2012) 32–34.
[50] S. Dahiya, R.M. Tripathi, A.G. Hegde, Biosorption of heavy metals and radionuclide from aqueous solutions by pre-treated arca shell biomass, J. Hazard. Mater., 150 (2008) 376–386.
[51] K.Y. Lee, M. Park, J. Kim, M. Oh, E.H. Lee, K.W. Kim, D.Y. Chung, J.K. Moon, Equilibrium, kinetic and thermodynamic study of cesium adsorption onto nanocrystalline mordenite from high-salt solution, Chemosphere, 150 (2016) 765–771.
[52] D.H. Ding, Y.X. Zhao, S.J. Yang, W.S. Shi, Z.Y. Zhang, Z.F. Lei, Y.N. Yang, Adsorption of cesium from aqueous solution using agricultural residue-walnut shell: equilibrium, kinetic and thermodynamic modeling studies, Water Res., 47 (2013) 2563–2571.
[53] E. Oguz, M. Ersoy, Removal of Cu^{2+} from aqueous solution by adsorption in a fixed bed column and neural network modelling, Chem. Eng. J., 164 (2010) 56–62.
[54] S. Zafar, N. Khalid, M.L. Mirza, Potential of rice husk for the decontamination of silver ions from aqueous media, Sep. Sci. Technol., 47 (2012) 1793–1801.
[55] H. Ghassabzadeh, A. Mohadespour, M. Torab-Mostaedi, P. Zaheri, M.G. Maragheh, H. Taheri, Adsorption of Ag, Cu and Hg from aqueous solutions using expanded perlite, J. Hazard. Mater., 177 (2010) 950–955.
[56] T. Jintakosol, W. Nitayaphat, Adsorption of silver(I) from aqueous solution using chitosan/montmorillonite composite beads, Mater. Res., 19 (2016) 1114–1121.
[57] W. Nitayaphat, T. Jintakosol, Removal of silver(I) from aqueous solutions by chitosan/bamboo charcoal composite beads, J. Cleaner Prod., 87 (2015) 850–855.
[58] A. Sari, M. Tüzen, Adsorption of silver from aqueous solution onto raw vermiculite and manganese oxide-modified vermiculite, Microporous Mesoporous Mater., 170 (2013) 155–163.
[59] M. Zhang, R. Helleur, Y. Zhang, Ion-imprinted chitosan gel beads for selective adsorption of Ag^{+} from aqueous solutions, Carbohydr. Polym., 130 (2015) 206–212.